Hydrogen bonding networks and cooperativity effects in the aqueous solvation of trimethylene oxide and sulfide rings by microwave spectroscopy and computational chemistry

Weslley G. D. P. Silva and Jennifer van Wijngaarden*

Department of Chemistry, University of Manitoba, Winnipeg, Manitoba R3T 2N2, Canada

*Corresponding author: vanwijng@umanitoba.ca

Abstract

The intermolecular interactions responsible for the microsolvation of the highly flexible trimethylene oxide (TMO) and trimethylene sulfide (TMS) rings with one and two water (w) molecules were investigated using rotational spectroscopy (8–22 GHz) and quantum chemical calculations. The observed patterns of transitions are consistent with the most stable geometries of the TMO–w, TMO–$(w)_2$ and TMS–w complexes at the B2PLYP-D3(BJ)/aug-cc-pVTZ level and were confirmed using spectra of the ^{18}O isotopologue. Due to its effectively planar backbone, TMO offers one unique binding site for solvation while water can bind to the puckered TMS ring in either an *axial* or *equatorial* site of the heteroatom. In all clusters, the first water molecule binds in the σ_v symmetry plane of the ring monomer and serves as a hydrogen bond donor to the heteroatom. The second water molecule is predicted to form a cooperative hydrogen bonding network between the three moieties. Secondary C–H···O interactions are a key stabilizing influence in the trimers and also drive the preferred binding site in the TMS clusters with the *axial* binding site preferred in TMS–w and the *equatorial* form calculated to be more stable in the dihydrate. Using an energy partition scheme from symmetry-adapted perturbation theory for the O, S and Se containing mono- and dihydrates, the intermolecular interactions are revealed to be mainly electrostatic but the dispersive character of the contacts is enhanced with increasing size of the ring's heteroatom due to the key role of longer-range secondary interactions.

Introduction

Accurate descriptions of non-covalent interactions are critical to achieve a comprehensive understanding of the driving forces behind important chemical phenomena including self-assembly, molecular recognition and the formation of supramolecular entities.[1,2] As a first step in characterizing intermolecular interactions, key properties related to structure and dynamics can be derived from experimental studies of prototypical monomers and their complexes formed with partner molecules in supersonic jets.[1,3] Clusters in which the binding partner is water are of particular interest to model the first stages of aqueous solvation. A number of examples are found in the literature including studies of hydrates formed with linear species,[4,5] rings[6–8] or other small compounds including amines,[9,10] ethers,[11] thiols and alcohols.[12] When high-resolution spectroscopy and quantum chemical calculations are combined and applied to such clusters, a detailed picture of the preferred binding sites, geometry, dynamics and the fundamental nature of the non-covalent interactions on a microscopic scale begins to emerge.

Intermolecular interactions involving the four-membered rings trimethylene oxide (c-C_3H_6O)(TMO) and trimethylene sulfide (c-C_3H_6S)(TMS) add an additional degree of complexity as the free monomers themselves are known to undergo a large amplitude ring puckering motion.[13] In both cases, the underlying potential energy surfaces along this coordinate are known to be double-well potentials with two equivalent minima corresponding to a non-planar ring backbone. In TMO, the barrier to planarity (15.52(5) cm^{-1})[14] based on spectroscopic studies is well below the zero point energy resulting in an effectively planar geometry for the heavy atom backbone.[15–23] As a result, the two lone pairs of electrons on oxygen offer equivalent binding sites for a partner molecule as seen through experimental measurements of

the rotational spectrum of TMO complexes with Ar,[24] HF,[25] HCl[26] and H_2O.[27] In TMS, the barrier to ring planarity (274(2) cm^{-1})[28] is much higher by comparison and the ground state geometry is that of a flexed ring as confirmed by tunnelling splitting in the microwave and rotationally-resolved infrared spectrum.[28–31] As the ring backbone is puckered, the lone pairs on sulfur, which are oriented axially or equatorially to the ring, provide two potential binding sites for the partner molecule. This has been confirmed via the rotational spectra of TMS–HF[32] and TMS–HCl[33] which contain signatures due to two separate isomers. In addition to providing interesting model systems to probe the contribution of the heteroatom (O versus S) to the character of the non-covalent interaction, the TMO and TMS monomers afford the opportunity to investigate the degree to which the binding partner quenches the large amplitude motion of the ring which may lead to subtle changes in its effective geometry. While the common assumption is that monomer geometries are not disrupted upon complexation,[3] Ottaviani *et al*. suggested that a 3° deviation from planarity of the ring was discernable from the millimeterwave spectrum of TMO–water (TMO–w) using deuterium and ^{18}O enriched samples.[27]

We describe herein a comprehensive study of the non-covalent interactions occurring in a series of water complexes formed with TMO and TMS in an effort to deduce how the geometry of the ring and the identity of the heteroatom affect the binding sites upon microsolvation by one and two water molecules. Using Fourier transform microwave (FTMW) spectroscopy, we report the first experimental observation of TMO–$(w)_2$ and TMS–w including measurements with ^{18}O enriched water for confirmation of the assignments. Furthermore, we have extended the work of Ottaviani *et al.*[27] to the microwave region by measuring new transitions for TMO–w (and ^{18}O water) including the first observation of the ^{13}C isotopologues in natural

abundance. For the three complexes, the observed spectral patterns are consistent with quantum chemical models at the B2PLYP-D3(BJ) and *ab initio* MP2 levels of theory which are extended to include predictions for TMS-$(w)_2$ and the selenium containing analogs for comparison. To enhance our understanding of the physical origins of the non-covalent contacts responsible for each cluster, we employed multiple computational approaches including topological and energy decomposition methods.

Experimental methods

The rotational spectra of TMO–w, TMO–$(w)_2$ and TMS–w were measured using a chirped-pulse (cp) and a cavity-based Balle-Flygare (BF) type Fourier transform microwave (FTMW) spectrometer which have been described previously.[34,35] In each experiment, a gas mixture containing 1% of the monomer vapour from above a liquid sample of the compound (Sigma-Aldrich Canada) in neon (100–300 kPa) was prepared at room temperature and seeded with water by passing it through a glass reservoir containing water or ^{18}O enriched water (97%). The gas mixture was expanded into the high vacuum chambers using a pulsed nozzle (1 mm orifice) to create a rotationally-cooled, supersonic jet expansion. Broadband cp-FTMW spectra were initially recorded in 2 GHz segments from 8–18 GHz from which the most intense rotational transitions for the parent species of the complexes were identified. In the case of the TMO–w dimer, the spectral features were sufficiently intense to also observe sets of transitions consistent with the corresponding ^{13}C isotopologues in natural abundance. Once a preliminary fit was obtained from the broadband spectrum, final frequency measurements were performed using the BF-FTMW instrument from 8–22 GHz which affords higher resolution and sensitivity. As the molecular beam and

the resonator axis are coaxial in the BF-FTMW instrument, all rotational transitions appeared as doublets due to the Doppler effect. The measured transitions have linewidths of ~7 kHz (FWHM) and their positions were determined to within ~2 kHz.

Computational methods

Initial conformational searches for TMO–$(w)_n$, TMS–$(w)_n$ and TMSe–$(w)_n$ (n=1,2) complexes were carried out at the GFN2-xTB[36] level using the Conformer-Rotamer Ensemble Sampling Tool (CREST) available in the extended tight binding (xTB) program package.[37,38] Following the searches, optimization and harmonic frequency calculations were performed for all possible geometries using the density functional theory (DFT) B3LYP[39]-D3(BJ)[40,41] method with Dunning's aug-cc-pVTZ[42] basis sets. For the TMO and TMS complexes, the geometries with relative energies within 10 kJ mol^{-1} were then subjected to optimization and frequency calculations using the double-hybrid B2PLYP[43]-D3(BJ) and *ab initio* MP2[44] methods with the aug-cc-pVTZ and Ahlrichs' def-2TZVP[45] basis set. The Boys and Bernardi's counterpoise correction method[46] was included in all optimization and frequency calculations to account for the basis set superposition error (BSSE). All optimization and frequency calculations were performed using the Gaussian 16 program.[47]

To visualize and quantify intermolecular interactions in the complexes, non-covalent interaction (NCI) and quantum theory of atoms in molecules (QTAIM) analyses were done using the NCIPLOT[48] and AIMAll[49] programs, respectively. Symmetry-adapted perturbation theory (SAPT) at the sapt2+(3)δMP2[50]/aug-cc-pVTZ was performed using the Psi4[51] to comprehend the physical origins of the interactions behind the formation of the complexes.

Results

A summary of the relative energies and spectroscopic parameters of the mono- and dihydrated complexes of TMO and TMS at the B2PLYP-D3(BJ) level is provided in Table 1 while the results from MP2 calculations are given in Table S13. The corresponding equilibrium structures for the lowest energy forms are presented in Figure 1 (monohydrates) and Figure 2 (dihydrates). As reported earlier by Ottaviani *et al*.,[27] the optimized geometry of TMO–w is heavily dependent on the level of theory employed with DFT calculations identifying a near planar TMO subunit with one binding site at oxygen to form a O···H–O hydrogen bond (HB) with water in the *ac*-plane of the TMO monomer and MP2 calculations predicting a TMO ring that is puckered by ~18º with two potential binding sites. This discrepancy is a result of the flatness of the potential energy surface along the TMO ring puckering coordinate and highlights the challenge of modelling compounds of this type. For the TMO–$(w)_2$ trimer (Figure 2), the second water molecule binds on the same side of the TMO ring (in the *ac*-plane of the monomer) and is oriented as a HB donor to the first.

As expected from studies of related weakly bound dimers with TMS,[32,33] the quantum chemical results for TMS–w identify two potential binding sites (*axial* and *equatorial*, Figure 1) in the *ac*-plane of the puckered ring monomer to form a S···H–O interaction with the former being slightly lower in energy. In this case, *axial* and *equatorial* designation refer to the orientation of the lone pair on S which can be intuited by analogy to the position of the H atom on the opposite side of the puckered TMS ring. Interestingly, in the TMS–$(w)_2$ trimer (Figure 2), by comparison, the lowest energy arrangement involves *equatorial* binding of the first water to sulfur with the second arranged as in the TMO analogue.

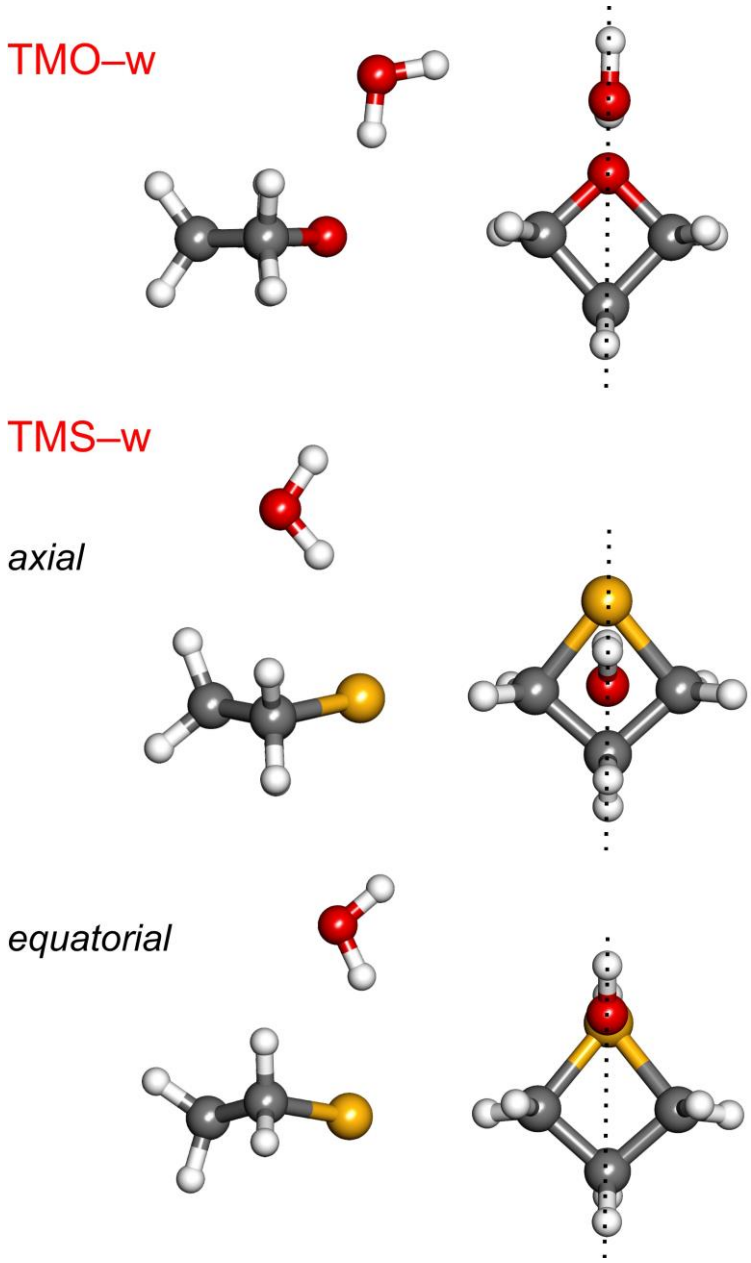

Figure 1. Equilibrium geometries (B2PLYP/aug-cc-pVTZ) of the conformers of TMO–w and TMS–w from a side (left) and a top (right) view. In the side view, the monomer *ac*-plane is in the plane of the page while in the top this plane is represented by a dotted line. The axial and equatorial binding sites of TMS-w refer to the orientation of the lone pair on S which is analogous to that of the H atom on the opposite side of the ring.

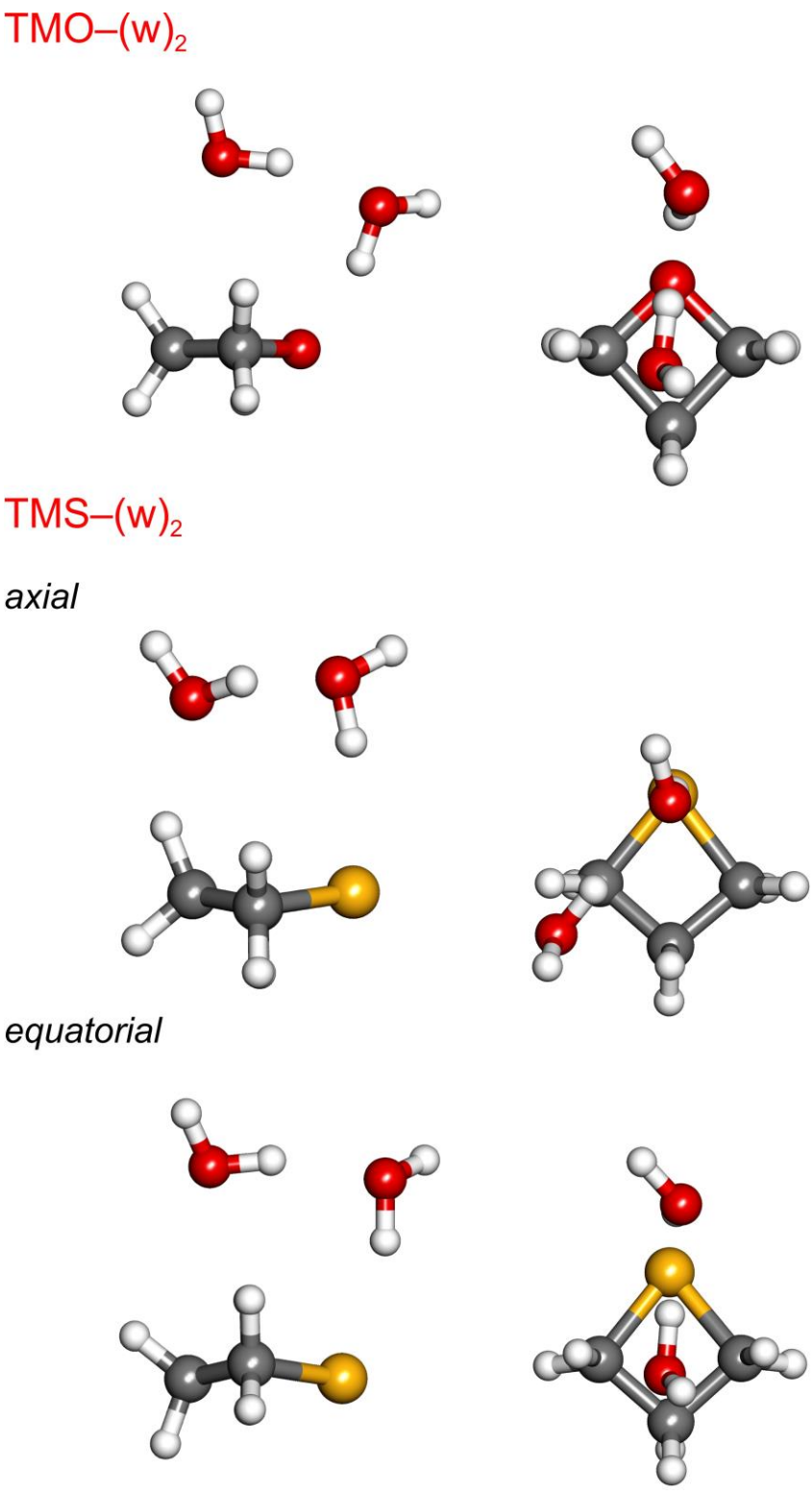

Figure 2. Equilibrium geometries (B2PLYP/aug-cc-pVTZ) of the conformers of TMO–$(w)_2$ and TMS–$(w)_2$ from a side (left) and a top (right) view.

Table 1. Calculated relative energies and spectroscopic parameters for the conformers of the mono- and dihydrated complexes of TMO and TMS.

	TMO–w	TMO–$(w)_2$	TMS–w		TMS–$(w)_2$	
Parameter[a]			*axial*	*equatorial*	*axial*	*equatorial*
A/MHz	8415/8151[b]	3559/3522	4389/4401	4640/4638	2784/2760	2697/2701
B/MHz	2624/2628	2042/2027	2522/2514	2365/2366	1505/1507	1675/1653
C/MHz	2444/2470	1608/1589	2223/2219	2152/2151	1210/1204	1264/1251
$\lvert\mu_a\rvert$/D	2.1/2.1	0.6/0.5	0.8/0.7	0.7/0.6	0.2/0.0	0.3/0.4
$\lvert\mu_b\rvert$/D	0.0/0.0	0.1/0.0	0.3/0.1	0.2/0.1	0.0/0.3	0.3/0.1
$\lvert\mu_c\rvert$/D	0.4/0.5	0.4/0.4	0.0/0.0	0.0/0.0	0.5/0.5	0.5/0.5
Complexation energy/kJ mol^{-1}	-29.4/-28.2	-68.4/-68.2	-23.8/-23.1	-23.1/-22.3	-57.5/-58.2	-59.0/-59.3
ΔE_{ZPE}/kJ mol^{-1}	—	—	0.0/0.0	0.7/0.8	1.1/1.0	0.0/0.0

[a]Rotational constants (*A*, *B* and *C*), absolute electric dipole moment components ($\lvert\mu_a\rvert$, $\lvert\mu_b\rvert$ and $\lvert\mu_c\rvert$), complexation energies accounting for basis set superposition errors and relative ZPE-corrected electronic (ΔE_{ZPE}) energies; [b]B2PLYP-D3(BJ), aug-cc-pVTZ/def2-TZVP basis set.

Based on the predicted spectroscopic parameters from Table 1, rotational transitions for the most stable conformers of TMO–$(w)_2$ and TMS–w were observed for the first time using both normal and ^{18}O enriched water samples. In the experiments involving gas mixtures with TMO, additional transitions due to TMO–w and its two singly substituted ^{13}C species in natural abundance were also assigned using the millimeterwave spectrum of the parent as a guide.[27] For this dimer, the ^{13}C transitions exhibited a relative intensity ratio of ~2:1 (C_α:C_β) due to the equivalence of the two α carbon atoms in the complex by symmetry. There was insufficient signal to detect the minor isotopologues of TMO–$(w)_2$ and TMS–w in natural abundance as the overall transition intensities were nearly two orders of magnitude lower than for TMO–w as shown in Figure 3. Each set of rotational transitions were fit independently with Pickett's SPFIT program[52] using Watson's S-reduced Hamiltonian (I^r representation).[53] The determined spectroscopic parameters for TMO–w are provided in Table S14 while those for TMO–$(w)_2$ and TMS–w are shown in Table 2. The transition frequencies from the BF-FTMW measurements are listed in Tables S15–S17.

In an effort to observe transitions arising from the *equatorial* conformer of TMS–w, as reported for the dimers with HF[32] and HCl,[33] the cp-FTMW spectrum was recorded with helium as the carrier gas. Although this form is only slightly higher in energy (0.5–0.7 kJ mol^{-1}, Table 1), no candidate lines corresponding to the *equatorial* conformer were observed. This may be a consequence, to some extent, of the smaller *a*-dipole but likely indicates that relaxation to the lower energy *axial* form is feasible.

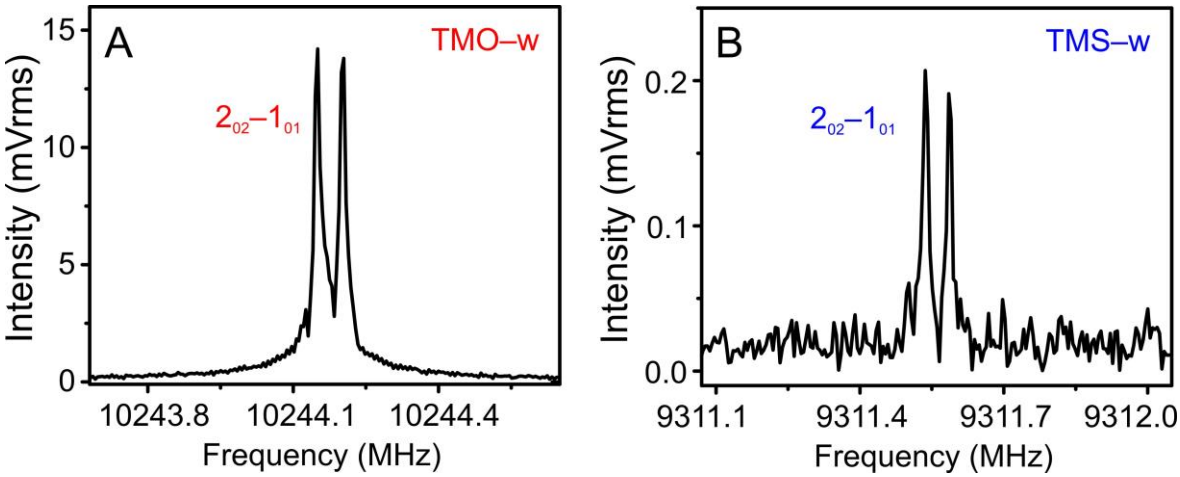

Figure 3. Cavity BF-FTMW spectrum for the J_{KaKc}' – J_{KaKc}" = 2_{02} – 1_{01} transition observed for A) TMO–w, 20 cycles and B) TMS–w, 220 cycles.

Using the rotational constants for the observed isotopologues of TMO–w and TMS–w, substitution coordinates (r_s) were derived using Kraitchman's equations[54] as implemented in the KRA routine.[55] For TMO–w, experimental information for the ^{13}C (this work) and deuterium isotopologues were available but were insufficient to derive the ring geometry without substitution at the position of the heteroatom. The labelled $H_2{}^{18}O$ sample, however, made it possible to experimentally confirm the position of water within the hydrated clusters both in the inertial frame of the complex and in the reference frame of the monomer. The latter was achieved by treating the water as a

point mass (18.01056 amu) relative to the ring. A comparison between the calculated and substituted coordinates is provided in Table S19.

Table 2. Spectroscopic parameters for the assigned conformers of TMO–$(w)_2$ and TMS–w

Parameter[a]	TMO–$(w)_2$		TMS–w	
	Parent	^{18}O	Parent	^{18}O
A/MHz	3487.4632(91)	3304.9560(82)	4427.9958(52)	4427.168(70)
B/MHz	2015.34068(93)	1916.26887(79)	2474.9504(16)	2323.79959(72)
C/MHz	1572.87970(60)	1476.30949(56)	2194.9170(14)	2074.92694(71)
D_J/kHz	1.7636(81)	1.5674(79)	5.178(22)	4.671(18)
D_{JK}/kHz	13.695(64)	12.944(65)	61.02(16)	58.47(53)
d_1/kHz	-0.3733(70)	-0.3491(65)	-0.576(29)	-0.482(12)
d_2/kHz	-0.0148(55)	-0.0397(56)	0.411(28)	0.351(26)
N	13	16	12	10
σ/kHz	1.7	2.0	2.4	0.9
$\mu_a/\mu_b/\mu_c$	y/n/n	y/n/n	y/y/n	y/n/n
P_{aa}/amu Å^2	213.59	226.58	160.16	173.45
P_{bb}/amu Å^2	107.73	115.76	70.10	70.12
P_{cc}/amu Å^2	37.19	37.16	44.04	44.03

[a]Rotational constants (*A*, *B* and *C*), quartic centrifugal distortion constants (D_J, D_{JK}, d_1, d_2), number of fitted transitions (*N*), standard deviation of the fit (σ); electric dipole moment components $\mu_a/\mu_b/\mu_c$ "y" if transitions related to the dipole were observed and "n" if not observed; planar moments of inertia (P_{aa}, P_{bb} and P_{cc}) obtained based on the rotational constants. The fitting was done using the transition frequencies from the BF-FTMW measurements.

Discussion

The experimentally-derived rotational constants of the TMO–w, TMO–$(w)_2$ and TMS–w complexes are consistent with the lowest energy geometries predicted at the B2PYLP level of theory with both aug-cc-pVTZ and def2-TZVP basis sets in Table 1 and with the results from MP2 calculations (Table S13) (with the exception of TMO–w

as mentioned above). The successful observation of transitions related to minor isotopic species based on these equilibrium geometries confirms that the effectively planar geometry of TMO and the puckered geometry of TMS (dihedral ∠C–C–C–S of ~18º) is retained following complexation with water. In the monohydrated clusters (Figure 1), the water molecule is positioned in the *ac*-plane (σ_v) of the heterocycle as supported by the close agreement between the planar moments associated with this plane (P_{bb}) in the TMO (36.99 amu Å^2)[20] and TMS (43.98 amu Å^2)[30] monomers and those corresponding to P_{cc}, the mirror plane of the TMO–w (36.89 amu Å^2) and TMS–w (44.04 amu Å^2) dimers in Figure 1. Further confirmation that the first water lies in the *ac*-plane of the TMO and TMS rings comes from the substitution coordinates in Table S20 which show that the center of mass of water has an imaginary *b*-coordinate (implying a near zero value).[56] In the TMO–$(w)_2$ trimer, the slightly larger P_{cc} value (37.19 amu Å^2) relative to that of TMO–w is consistent with the slight rotation of the first water molecule in the trimer to move one hydrogen out of the symmetry plane as seen in Figure 2. This slight re-orientation presumably stabilizes the HB formed between the two water molecules.

Key information regarding the stability of the TMO–w and TMS–w dimers can be extracted from the QTAIM molecular graphs in Figure 4 that represent the non-covalent interactions as bond paths (black solid or dashed lines) between atoms. The primary contact in TMO–w is approximately three times stronger than the sulfur HB in TMS–w. This highlights the weaker acceptor character of sulfur compared to that of oxygen and is consistent with the distances between the center of mass of water and the S (3.38 Å) or O (2.87 Å) heteroatoms of the ring from the Kraitchman analysis (adopting the equilibrium monomer geometries of TMO and TMS from B2PLYP/aug-cc-pVTZ calculations). The puckered geometry of TMS, however, permits the

establishment of a secondary contact in TMS–w with a stabilizing energy of ~5.0 kJ mol^{-1} from the QTAIM results and is confirmed in the NCI calculations (Figure 4) by the presence of a green isosurface between C$_\beta$–H and the O of water. It is interesting to note that although the *axial* conformer of TMS–w is ~0.5–0.7 kJ mol^{-1} (Table 1) more stable than the *equatorial* form, its dominant S···H–O interaction is slightly smaller by ~0.3 kJ mol^{-1} suggesting that the substantial secondary C$_\beta$–H···O contact is the determining factor for the preferred *axial* binding site in TMS–w. A similar experimental finding was reported for TMS dimers with HF[32] and HCl.[33]

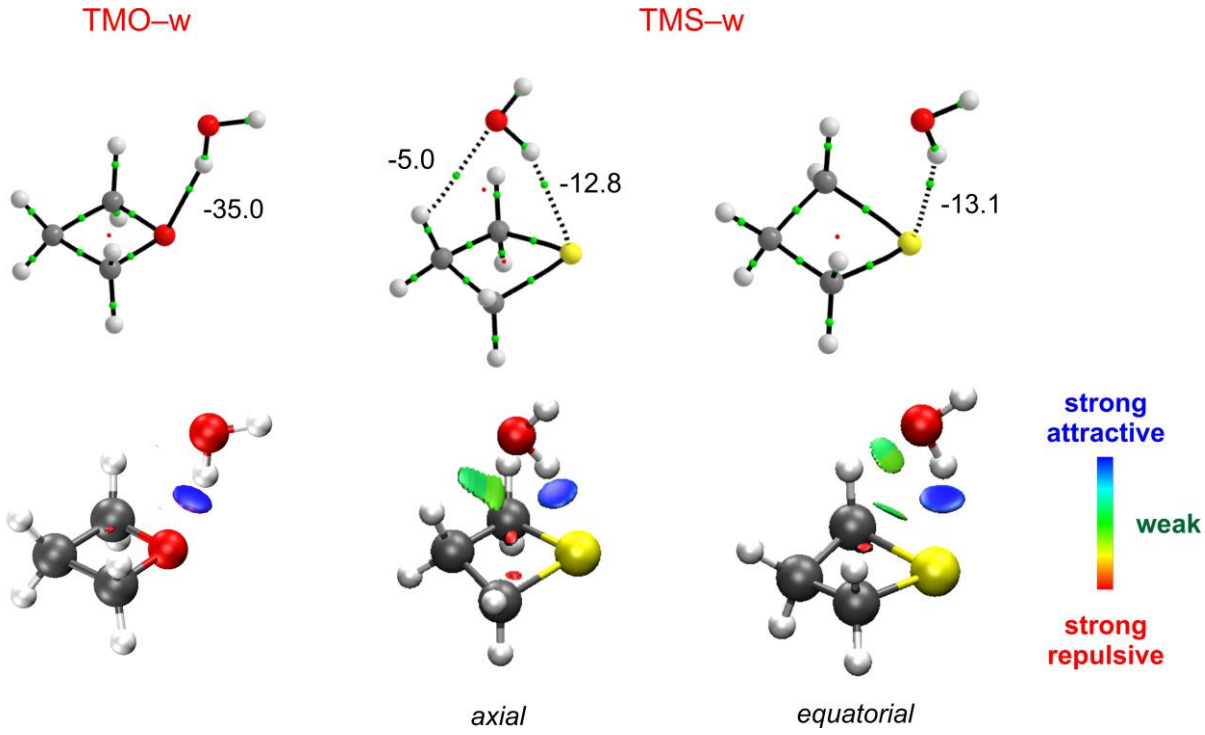

Figure 4. QTAIM molecular graphs (top) and NCI isosurfaces (bottom, *s*= 0.5, colour scale BGR -0.02 < ρ < +0.02) for the conformers of the TMO–w and TMS–w

In moving to the dihydrated clusters (Figure 5), the topology of the HB interactions is significantly altered to accommodate the additional water molecule. While the first water serves as a HB donor to the ring heteroatom to form O···H–O or S···H–O primary interactions, it also acts as a HB acceptor for the second water molecule as depicted in Figure 5. In turn, the second water acts as both donor and

acceptor as it binds to the first via O···H–O HB interactions and to the methylene groups of the rings through smaller secondary Cβ–H···O contacts. The intermolecular contacts established between the three components are examples of cooperative HB networks as observed for other water complexes.[11,57] The result is the strengthening of the primary contact by more than 10 kJ mol^{-1} relative to the corresponding dimers due to the decreased HB distances (~0.1Å (B2PLYP-D3(BJ)/aug-cc-pVTZ) shorter for both trimers). Note that the primary interaction is more pronounced in the TMO trimers than in the TMS trimers which is consistent with the weaker acceptor character of sulfur.

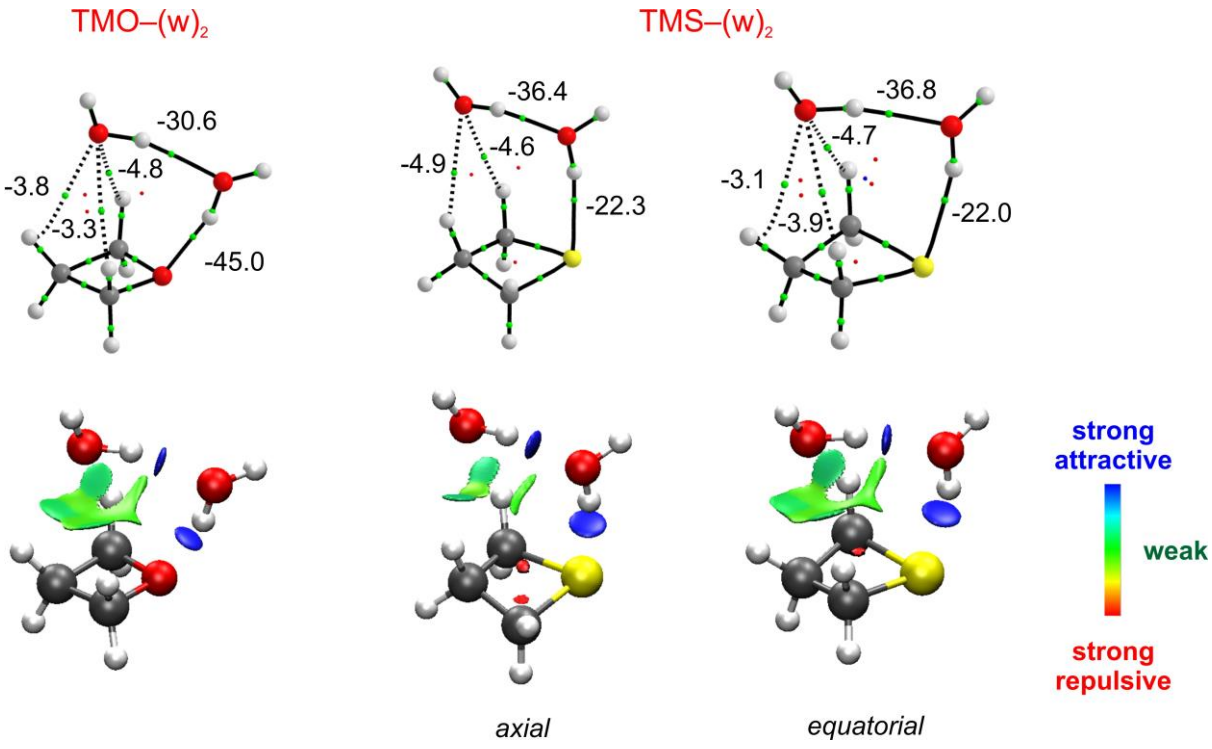

Figure 5. QTAIM molecular graphs (top) and NCI isosurfaces (bottom, *s*= 0.5, colour scale BGR -0.02 < ρ < +0.02) for the conformers of the TMO–(w)$_2$ and TMS–(w)$_2$

While the *axial* binding site was preferred in the TMS–w dimer, a surprising change is predicted in the relative energy ordering of the TMS–(w)$_2$ as the *equatorial*

form is ~1 kJ mol^{-1} (Table 1) more favourable. As seen in Figure 5, this increased stability is due to the three weak contacts established between the second water and the methylene hydrogen atoms. In the *axial* conformer by comparison, the second water is not centered on the *ac*-plane of the TMS ring and forms non-covalent interactions with only two C–H groups (Figures 2 and 5). This key difference in the position of the second water is captured using the rotational constants based on the equilibrium geometries from Table 1 (B2PLYP/aug-cc-pVTZ) to estimate the P_{cc} values for the *axial* (49.83 amu $Å^2$) and *equatorial* (44.64 amu $Å^2$) conformers of TMS–$(w)_2$, which show that, in the *equatorial* form, the second water molecule is more centered over the ring and close to the symmetry plane of the TMS monomer (43.98 amu $Å^2$) and TMS–w (44.04 amu $Å^2$) dimer.

Finally, SAPT calculations provide deeper insights regarding the nature of the intermolecular interactions as the interaction energies are partitioned in terms of electrostatic, dispersive, inductive and exchange-repulsive components. In Table 3, SAPT results for the TMO, TMS, and TMSe hydrates are provided to evaluate the effect of the chalcogen atom on the stability of the complexes. As in the TMS clusters, the two most stable geometries of the Se containing complexes are predicted to adopt both *axial* and *equatorial* configurations (Figure S1) with the former being the most stable monohydrate and the latter favoured in the presence of two waters. For all complexes, the total interaction energies show a stability ordering of O > S > Se in accordance with the non-covalent interaction strengths derived from the QTAIM analysis (Figure 4, Figure 5 and Figure S1 for the Se derivatives). From the partitioned energies, the electrostatic term is the main contributor to the stability of all clusters, but its role diminishes as the size of the heteroatom increases and this trend is partially offset by an increase in the % contribution from dispersion. This is particularly true for

the monohydrates of the S and Se heterocycles which exhibit the longer range C_β–H···O contacts due to the puckered geometry of the ring. Although these secondary interactions are smaller than the primary HB with the heteroatom of the ring, they clearly drive the energetic preference for the *axial* form of TMS-w and TMSe–w and the *equatorial* conformers of TMS–$(w)_2$ and TMSe–$(w)_2$.

Table 3. SAPT results (in kJ mol^{-1}) for the mono- and dihydrates of TMO, TMS and TMSe obtained at the SAPT2+(3)δMP2/aug-cc-pVTZ level of theory.

Complex	Electrostatic	Induction	Dispersion	Exchange	Total
TMO–w	-44.1 (57.0)[a]	-16.3 (21.1)	-17.0 (22.0)	48.0	-29.4
TMO–$(w)_2$	-63.1 (54.4)	-25.6 (22.1)	-27.3 (23.5)	67.2	-48.9
TMS–w *axial*	-31.9 (51.9)	-12.4 (20.2)	-17.2 (28.0)	38.1	-23.4
TMS–w *equatorial*	-29.3 (50.7)	-11.9 (20.6)	-16.6 (28.7)	34.8	-23.0
TMS–$(w)_2$ *axial*	-47.1 (50.6)	-21.7 (23.3)	-24.3 (26.1)	56.4	-36.7
TMS–$(w)_2$ *equatorial*	-48.0 (49.0)	-23.2 (23.7)	-26.8 (27.3)	58.9	-39.1
TMSe–w *axial*	-30.0 (51.2)	-11.9 (20.3)	-16.7 (28.5)	36.3	-22.4
TMSe–w *equatorial*	-28.3 (49.3)	-11.8 (20.5)	-17.3 (30.2)	35.3	-22.1
TMSe–$(w)_2$ *axial*	-46.0 (49.6)	-22.2 (23.9)	-24.6 (26.5)	57.0	-35.7
TMSe–$(w)_2$ *equatorial*	-45.6 (48.2)	-22.5 (23.8)	-26.4 (27.9)	56.6	-37.9

[a]Values in brackets ( ) represent the contribution of that term (in percentage) to the total stabilizing energy (electrostatic + induction + dispersion).

Conclusions

The factors governing the aqueous microsolvation of the four-membered heterocycles TMO and TMS were explored using FTMW spectroscopy and quantum chemistry. The establishment of intermolecular contacts with water does not appear to have a discernable effect on the geometry of the ring monomers and the preferred

binding sites for the solvent depend on the capacity to form primary and secondary HB contacts with the heteroatom and methylene groups of the ring, respectively. The latter interactions were found to be a strong influence on the position of water in the TMS containing clusters due to its puckered ring geometry. For the dihydrated rings, cooperative hydrogen bonding networks identified through QTAIM calculations provide additional stability for the clusters through an increase of the primary HB contacts by more than 10 kJ mol^{-1} and through formation of additional secondary HB contacts which were confirmed by NCI calculations. SAPT analysis captures the nature of these secondary interactions as an increase in the % dispersion character and also confirms that the greater stability of the TMO complexes over those formed with the S (and Se) analogues is due to greater electrostatic contributions to the interaction energy. These seemingly small but significant differences highlight the importance of modelling the stepwise solvation of flexible molecules and the central role of long-range interactions in driving this process.

Supplementary Material

Appendix 1: Cartesian coordinates for the conformers of the studied complexes

Appendix 2: Calculated spectroscopic parameters for the TMO and TMS mono- and dihydrates at the MP2 level

Appendix 3: Fitted parameters and observed transition frequencies for the assigned conformers of TMO–w, TMO–$(w)_2$ and TMS–(w)

Appendix 4: Calculated rotational and centrifugal distortion constants for the observed conformers obtained at the B2PLYP-D3(BJ) level of theory

Appendix 5: Kraitchman analysis for TMO–w and TMS–w

Appendix 6: QTAIM and NCI results for the TMSe mono- and dihydrates

Acknowledgements

We acknowledge the Natural Sciences and Engineering Research Council of Canada (NSERC) for funding this research through the Discovery Grant program and the University of Manitoba for its computational research facility, GREX. W.G.D.P.S is also grateful for a University of Manitoba Graduate Fellowship (UMGF) provided by the Faculty of Graduate Studies.

Data Availability Statement

The data that supports the findings of this study are available within the article and its supplementary material.

References

[1] M. Juanes, R.T. Saragi, W. Caminati, and A. Lesarri, Chem. – A Eur. J. **25**, 11402 (2019).

[2] S.J. Grabowski, Chem. Rev. **111**, 2597 (2011).

[3] Y. Xu, J. van Wijngaarden, and W. Jäger, Int. Rev. Phys. Chem. **24**, 301 (2005).

[4] A.J. Barclay, A. Pietropolli Charmet, A.R.W. McKellar, and N. Moazzen-Ahmadi, J. Chem. Phys. **154**, (2021).

[5] A.S. Bogomolov, A. Roucou, R. Bejjani, M. Herman, N. Moazzen-Ahmadi, and C. Lauzin, Chem. Phys. Lett. **774**, 138606 (2021).

[6] R.B. Mackenzie, C.T. Dewberry, R.D. Cornelius, C.J. Smith, and K.R. Leopold, J. Phys. Chem. A **121**, 855 (2017).

[7] W.G.D.P. Silva and J. van Wijngaarden, J. Phys. Chem. A **125**, 3425 (2021).

[8] J. Wang, L. Spada, J. Chen, S. Gao, S. Alessandrini, G. Feng, C. Puzzarini, Q. Gou,

J. Grabow, and V. Barone, Angew. Chemie Int. Ed. **58**, 13935 (2019).

[9] W.G.D.P. Silva, T. Poonia, and J. van Wijngaarden, Phys. Chem. Chem. Phys. **23**, 7368 (2021).

[10] J. Chen, Y. Zheng, A. Melli, L. Spada, T. Lu, G. Feng, Q. Gou, V. Barone, and C. Puzzarini, Phys. Chem. Chem. Phys. **22**, 5024 (2020).

[11] M. Fatima, D. Maué, C. Pérez, D.S. Tikhonov, D. Bernhard, A. Stamm, C. Medcraft, M. Gerhards, and M. Schnell, Phys. Chem. Chem. Phys. **22**, 27966 (2020).

[12] M. Juanes, R.T. Saragi, R. Pinacho, J.E. Rubio, and A. Lesarri, Phys. Chem. Chem. Phys. **22**, 12412 (2020).

[13] A.C. Legon, Chem. Rev. **80**, 231 (1980).

[14] J. Jokisaari and J. Kauppinen, J. Chem. Phys. **2260**, 2260 (1973).

[15] J. Fernandez, R.J. Myers, and W.D. Gwinn, J. Chem. Phys. **23**, 758 (1955).

[16] S.I. Chan, J. Zinn, J. Fernandez, and W.D. Gwinn, J. Chem. Phys. **33**, 1643 (1960).

[17] S.I. Chan, T.R. Borgers, J.W. Russell, H.L. Strauss, and W.D. Gwinn, J. Chem. Phys. **44**, 1103 (1966).

[18] R.A. Creswell and I.M. Mills, J. Mol. Spectrosc. **52**, 392 (1974).

[19] R.A. Creswell, Mol. Phys. **30**, 217 (1975).

[20] A. Lesarri, S. Blanco, and J.C. López, J. Mol. Struct. **354**, 237 (1995).

[21] M. Winnewisser, M. Kunzmann, M. Lock, and B. Winnewisser, J. Mol. Struct. **561**, 1 (2001).

[22] G. Moruzzi, M. Kunzmann, B.P. Winnewisser, and M. Winnewisser, J. Mol. Spectrosc. **219**, 152 (2003).

[23] O. Mahassneh and J. van Wijngaarden, J. Mol. Spectrosc. **371**, (2020).

[24] F. Lorenzo, A. Lesarri, J.C. Lopez, and J.L. Alonso, Chem. Phys. Lett. **286**, 272 (1998).

[25] M.E. Sanz, V.M. Sanz, J.C. López, and J.L. Alonso, Chem. Phys. Lett. **342**, 31 (2001).

[26] S. Antolínez, J.C. López, and J.L. Alonso, Chem. Phys. Lett. **334**, 250 (2001).

[27] P. Ottaviani, M. Giuliano, B. Velino, and W. Caminati, Chem. - A Eur. J. **10**, 538 (2004).

[28] D.O. Harris, H.W. Harrington, A.C. Luntz, and W.D. Gwinn, J. Chem. Phys. **44**, 3467 (1966).

[29] M.S. White and E.L. Beeson, J. Chem. Phys. **43**, 1839 (1965).

[30] R. Hinze, A. Guarnieri, J.L. Alonso, and J.C. López, J. Mol. Struct. **350**, 195 (1995).

[31] J. van Wijngaarden, D. Desmond, and W. Leo Meerts, J. Mol. Spectrosc. **315**, 107 (2015).

[32] M.E. Sanz, J.C. López, and J.L. Alonso, Chem. - A Eur. J. **8**, 4265 (2002).

[33] M.E. Sanz, A. Lesarri, J.C. López, and J.L. Alonso, Angew. Chemie Int. Ed. **40**, 935 (2001).

[34] L. Evangelisti, G. Sedo, and J. van Wijngaarden, J. Phys. Chem. A **115**, 685 (2011).

[35] G. Sedo and J. van Wijngaarden, J. Chem. Phys. **131**, 044303 (2009).

[36] C. Bannwarth, S. Ehlert, and S. Grimme, J. Chem. Theory Comput. **15**, 1652 (2019).

[37] P. Pracht, F. Bohle, and S. Grimme, Phys. Chem. Chem. Phys. **22**, 7169 (2020).

[38] S. Grimme, J. Chem. Theory Comput. **15**, 2847 (2019).

[39] A.D. Becke, J. Chem. Phys. **98**, 5648 (1993).

[40] S. Grimme, J. Antony, S. Ehrlich, and H. Krieg, J. Chem. Phys. **132**, 154104 (2010).

[41] S. Grimme, S. Ehrlich, and L. Goerigk, J. Comput. Chem. **32**, 1456 (2011).

[42] T.H. Dunning, J. Chem. Phys. **90**, 1007 (1989).

[43] S. Grimme, J. Chem. Phys. **124**, 034108 (2006).

[44] C. Møller and M.S. Plesset, Phys. Rev. **46**, 618 (1934).

[45] F. Weigend and R. Ahlrichs, Phys. Chem. Chem. Phys. **7**, 3297 (2005).

[46] S.F. Boys and F. Bernardi, Mol. Phys. **19**, 553 (1970).

[47] M. J. Frisch, G. W. Trucks, H. B. Schlegel, G. E. Scuseria, M. A. Robb, J. R. Cheeseman, G. Scalmani, V. Barone, G. A. Petersson, H. Nakatsuji, X. Li, M. Caricato, A. V. Marenich, J. Bloino, B. G. Janesko, R. Gomperts, B. Mennucci, H. P. Hratchian, J. V. Ortiz, A. F. Izmaylov, J. L. Sonnenberg, D. Williams-Young, F. Ding, F. Lipparini, F. Egidi, J. Goings, B. Peng, A. Petrone, T. Henderson, D. Ranasinghe, V. G. Zakrzewski, J. Gao, N. Rega, G. Zheng, W. Liang, M. Hada, M. Ehara, K. Toyota, R. Fukuda, J. Hasegawa, M. Ishida, T. Nakajima, Y. Honda, O. Kitao, H. Nakai, T. Vreven, K. Throssell, J. A. Montgomery, Jr., J. E. Peralta, F. Ogliaro, M. J. Bearpark, J. J. Heyd, E. N. Brothers, K. N. Kudin, V. N. Staroverov, T. A. Keith, R. Kobayashi, J. Normand, K. Raghavachari, A. P. Rendell, J. C. Burant, S. S. Iyengar, J. Tomasi, M. Cossi, J. M. Millam, M. Klene, C. Adamo, R. Cammi, J. W. Ochterski, R. L. Martin, K. Morokuma, O. Farkas, J. B. Foresman, and D. J. Fox, Gaussian 16, Revision C.01, Gaussian, Inc., Wallingford, CT, 2016

[48] J. Contreras-García, E.R. Johnson, S. Keinan, R. Chaudret, J.-P. Piquemal, D.N. Beratan, and W. Yang, J. Chem. Theory Comput. **7**, 625 (2011).

[49] T.A. Keith, AIMAll, Version 17.11.14, TK Gristmill Software, Overland Park, KS, 2013.

[50] E.G. Hohenstein and C.D. Sherrill, J. Chem. Phys. **133**, 014101 (2010).

[51] R.M. Parrish, L.A. Burns, D.G.A. Smith, A.C. Simmonett, A.E. DePrince, E.G. Hohenstein, U. Bozkaya, A.Y. Sokolov, R. Di Remigio, R.M. Richard, J.F. Gonthier, A.M. James, H.R. McAlexander, A. Kumar, M. Saitow, X. Wang, B.P. Pritchard, P. Verma, H.F. Schaefer, K. Patkowski, R.A. King, E.F. Valeev, F.A. Evangelista, J.M. Turney, T.D. Crawford, and C.D. Sherrill, J. Chem. Theory Comput. **13**, 3185 (2017).

[52] H.M. Pickett, J. Mol. Spectrosc. **148**, 371 (1991).

[53] J.K.G. Watson, J. Chem. Phys. **48**, 4517 (1968).

[54] J. Kraitchman, Am. J. Phys. **21**, 17 (1953).

[55] Z. Kisiel, in *Spectroscopy from Space*, edited by J. Demaison et al. (Kluwer Academic Publishers, Dordrecht, 2001), pp. 91–106.

[56] W. Gordy, and R.L. Cook, *Microwave Molecular Spectra*, 3rd edition (John Wiley & Sons Inc., New York, 1984).

[57] D. Loru, A.L. Steber, P. Pinacho, S. Gruet, B. Temelso, A.M. Rijs, C. Pérez, and M. Schnell, Phys. Chem. Chem. Phys. **23**, 9721 (2021).